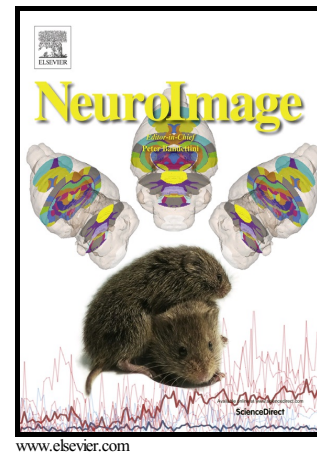


Monitoring Cardiac and Respiratory Physiology
During FMRI

Daniel Bulte, Karolina Wartolowska



PII: S1053-8119(16)30692-9
DOI: <http://dx.doi.org/10.1016/j.neuroimage.2016.12.001>
Reference: YNIMG13622

To appear in: *NeuroImage*

Received date: 13 July 2016
Revised date: 28 November 2016
Accepted date: 1 December 2016

Cite this article as: Daniel Bulte and Karolina Wartolowska, Monitoring Cardiac and Respiratory Physiology During FMRI, *NeuroImage* <http://dx.doi.org/10.1016/j.neuroimage.2016.12.001>

This is a PDF file of an unedited manuscript that has been accepted for publication. As a service to our customers we are providing this early version of the manuscript. The manuscript will undergo copyediting, typesetting, and review of the resulting galley proof before it is published in its final citable form. Please note that during the production process errors may be discovered which could affect the content, and all legal disclaimers that apply to the journal pertain.

Monitoring Cardiac and Respiratory Physiology During FMRI

Daniel Bulte^{1,2}, Karolina Wartolowska³

¹Functional Magnetic Resonance Imaging of the Brain Centre Nuffield Department of Clinical Neurosciences University of Oxford. John Radcliffe Hospital, Oxford OX3 9DU, UK

²Institute of Biomedical Engineering Department of Engineering Science Old Road Campus Research Building University of Oxford Oxford OX3 7DQ, UK

³Botnar Research Centre Nuffield Department of Orthopaedics, Rheumatology and Musculoskeletal Sciences University of Oxford Old Road Oxford OX3 7LD, UK
daniel.bulte@ndcn.ox.ac.uk

Abstract

This article will consider how physiological monitoring can be used both as an intrinsic part of an experiment, or for removing unwanted physiological signals from the FMRI time series. As functional MRI is used for a wide variety of applications beyond the identification of regions involved in a task, different sources of noise in the time series become important. The use of arterial spin labelling sequences, either in isolation or combined with BOLD imaging, means that temporal noise must be dealt with differently. Moreover, when these are combined with global cerebrovascular stimuli, such as respiratory challenges, the standard analysis tools must be employed with great care so as not to detrimentally distort the data. Acquiring and analysing physiological data is sometimes more art than science, and this article attempts to provide some insight into common techniques as well as advice on identifying and correcting some of the problems that may be encountered.

Keywords: BOLD, ASL, oxygen, carbon dioxide, gas challenge, respiratory, cardiac, gating, calibrated FMRI.

Introduction

The story of functional MRI is one of the meticulous extraction of signal from noise, and often it has led to the surprising discovery that much of that noise was in fact signal as well. Volumes have been written on motion correction [1, 2], independent component analysis (ICA) [3, 4], unwarping [5], and correcting for respiratory and cardiac phase [6, 7], and scientific careers have been made on the creation of user-friendly software for analysing the functional magnetic resonance (FMRI) time series (FSL, SPM, & AFNI). This article will focus on methods for collecting physiological data, types of data required for different paradigms or acquisition schemes, and how to best incorporate these data into analyses. The traditional task-based or event-related FMRI experiments still dominate the field; however, in recent years we have seen greater interest in low frequency responses such as resting state, imaging of state (for example, ongoing pain) or respiratory gas or breathing challenges. For a general overview of respiratory challenge MRI I would recommend the recent excellent paper by Moreton *et al.* [8]. The use of pulse sequences other than gradient echo blood oxygenation level depended

(BOLD) imaging has also become much more common, with different variants of arterial spin labelling (ASL) competing for dominance. Modelling these time series requires a different approach, and the temporal and spatial characteristics of these sequences significantly alters the interactions between the data and physiological signals. Much of the content of this article is the result of lessons learned and personal experience with different forms of physiological monitoring, and as such, it comes with examples rather than citations. For a refresher on oxygen transport and a crib sheet for the many acronyms used I recommend an article by Treacher and Leach [9].

Breathing artefacts

Motion correction might seem to be the most obvious correction to apply to functional imaging data; however, it is worth noting that dangers lie within complacency. Although there are excellent motion correction algorithms built into the major analysis software packages, the user still needs to exercise caution and understand what these tools can and cannot do, in particular, what kinds of errors the tools themselves may introduce. Motor tasks have always been a potential source of subject movement; however, the careful use of foam padding generally mitigates head motion related to finger-tapping tasks. Breathing is known to influence the BOLD signal, but this can be usually accounted for by the use of a respiratory belt (see the Physiological Signals section for a more detailed discussion of this). Data from fMRI studies incorporating breathing challenges however, can be notoriously difficult to acquire without significant motion artefacts. The problem with breathing-based tasks is that motion is correlated with the task. That is why experiments using hyperventilation, deep breathing, or breath holds may be affected by head-motion artefacts. In these cases, the naïve application of a motion correction tool can actually result in spurious activations. Most of the motion correction tools produce a report which provides a motion time series. It is essential to check this report for large, task-correlated motion. The other key sign that breathing-related artefacts have corrupted the data is the presence of boundary activations on the activation maps. These can be at grey/white matter boundaries, around the ventricles, or simply as a halo around the edge of the brain. This will become especially obvious if a group of subjects are registered to a standard brain, as the internal boundary

activations are likely to cancel out due to between-subject differences, whereas the outer-edge artefacts will tend to reinforce.

In the case of severe motion of a subject during a scan, particularly if the subject is considered “valuable” (i.e. a patient with a rare condition, or at an acute stage), it can be extremely frustrating that a time series may be rendered effectively useless by a poorly timed sneeze. In some of these cases the data may be rescued through the removal of the effect of the small number of volumes considered to be motion outliers from the analysis. This must be done carefully using an appropriate tool, or else the sudden loss of volumes will cause further errors in the analysis (see for example <http://fsl.fmrib.ox.ac.uk/fsl/fslwiki/FSLMotionOutliers>).

Physiological Signals

In most common forms of FMRI, the majority of the physiological information in the MR signal is noise. However, when attempting to measure physiology, there is a fine line between what is signal and what is noise. The subject may have multiple ancillary data acquisition devices connected to them in the scanner, all collecting physiological data, which may either be modelled out as a nuisance regressor, or be included in models as a critical aspect of the analysis. The most common strategy is to obtain data for RETROICOR-type corrections for physiological noise [6]. This approach uses cardiac and respiratory phase information to remove the influence of these physiological changes from the functional time series [7]. Usually, the respiratory data is collected using an elastic belt wrapped around the subject’s abdomen or chest to track the breathing motion in order to determine the end-inspiration and end-expiration points. The cardiac data is acquired using an infrared pulse oximeter in the shape of a finger clip, which monitors the heartrate via changes in blood volume (photoplethysmography). In addition to physiological data, we have to acquire the timing of the readout triggers from the scanner, as the physiological time series have to be used in sync with the FMRI data. The physiological data contains the information about the point in the respiratory and cardiac cycles at which the MRI volume has been collected. It is important to realise that RETROICOR-type approaches correct for *phase only*. These methods do not account for changes in respiratory rate, heart rate, or

arterial oxygen saturation (SaO_2), which can also affect fMRI data. Thus, if a subject hyperventilates or holds their breath during a task, thereby altering their arterial partial pressures of carbon dioxide (PaCO_2) and cerebral blood flow (CBF), it will not be corrected using these methods. CO_2 levels are relevant as they correlate with global CBF, and thus can scale both the BOLD and ASL response [10]. The respiratory belt data could be analysed to produce a respiration-rate time course, which theoretically should correlate with PaCO_2 , however, in practice the signal-to-noise ratio (SNR) of this method is too low to be reliable.

The relationship between respiration and the fMRI time series is complex. Breathing rate and depth has been shown to impact the BOLD response, most likely through changes in PaCO_2 [11]. It has been noted that apart from the random fluctuations in breathing that occur naturally over the course of an experiment, there is also a tendency for subjects' breathing to be affected by the tasks themselves [12, 13]. This effect seems to be greatest during motor tasks; however, some subjects increase their breathing rate while decreasing the depth during a motor task, the amplitude of which will correlate with the complexity of the task, while other subjects hold their breath while concentrating on a motor task. Each of these will impact the measurement of both the localisation and scale of activations. Again, this effect will not be accounted for by RETROICOR-type corrections as the effect is not dependent on the interaction of the task with breathing phase, but rather with breathing frequency. If these effects are of concern, the best solution may be to train subjects in advance to be more aware of their breathing while performing tasks, as task-correlated breathing patterns can be very difficult to regress out. Alternately, due to a variety of tasks and stimuli affecting breathing rate or depth; it may be beneficial to use visual or auditory cues as a metronome to regulate breathing when this is a concern.

It is becoming more common to continuously measure the oxygen and CO_2 levels in the respiratory gases during fMRI experiments. With an appropriate adjustment to account for the sampling delay, these data can be used directly as a regressor in the model. Every respiratory gas analysis system will have its own characteristic sampling delay. The length of sample tube and the power of the pump pulling the gas into the analysis device will determine how far out of synchronisation the scanner triggers and the

respiratory waveforms are. The simplest means of determining the delay in a system is to use an event marker and a breath-hold task. It is easiest to use the “breath-in” instruction as the event, and the CO₂ trace as the measurement, because the end-tidal point provides a sharper transition to measure the delay from. This is best to perform as a set of instructions: “breathe in”, “breathe out”, “breathe in and hold your breath” (this is the moment to set the marker), “breathe normally”. This short breath hold allows for the easy identification of the correct end-tidal point. The respiratory data can then be synchronised with the scanner triggers, resampled, and used as a regressor to analyse the FMR time series (see next section for more detail).

Similarly, pulse triggers can be analysed to create a time course of the heart rate for inclusion in the analysis [14]. In addition to providing a simple pulse trigger, more sophisticated fibre optic pulseoximeter devices can continuously monitor SaO₂ and heart rate. As breathing and respiratory gas challenges can alter PaCO₂ and SaO₂ and thus alter baseline values for BOLD, this may either introduce problematic noise, or be an essential aspect of the experiment. In the case of ASL in conjunction with hyperoxia, the increase in arterial partial pressure of oxygen (PaO₂) reduces the T₁ of arterial blood, which must be accounted for when calculating the CBF [15]. Using carbogen (a mix of 95% oxygen and 5% CO₂) and pseudo-continuous ASL (PCASL) is even more complicated as the increased PaO₂ alters the arterial T₁, while the CO₂ increases the flow velocity through the tagging arteries, reducing the inversion efficiency [15, 16]. (See BOLD and ASL section below for more details.)

The interaction between cardiac phase and ASL can also be significant. As the labelling efficiency of PCASL is partially determined by the arterial flow velocity through the tagging plane, the point in the cardiac cycle at which tagging occurs will impact labelling [17]. Over a large number of samples, this effect will average out with a similar number of labelling events spread between diastole and systole, however when using multiple post-labelling delay ASL, or if using single post-labelling delays with relatively short duration tasks, this averaging may not occur effectively. The impact of cardiac phase can be determined for a particular implementation or alternatively, there has been some promising work showing the effectiveness of using cardiac triggers to reduce the degree of variability of cardiac phase with tagging and read-outs [18]. This approach assumes

that the subject is not experiencing dramatic variations in heart rate during the scan, as there are multiple heartbeats between the labelling and the read-out.

Removing physiological noise from FMRI

An independent component analysis (ICA) can be used for decomposition of FMRI data into independent components with a common time series and a weighted set of voxels (the spatial map)[3]. These components can be classified as signal or noise and the noise components can be subsequently removed. In fact, the components may be classified as “signal”, “respiratory”, “cardiac”, “sagittal sinus”, “movement”, “thermal” etc. but, unless we are particularly interested in any of these components, all these are simply classified as “noise”.

The components related to physiological noise can be identified by “eyeballing” or using an algorithm based on their distinct characteristics. They tend to have an oscillatory, “zig-zag” time course (sharply and symmetrically alternating up and down without individual spikes) and clear peaks in the power spectrum of the time course. Moreover, the signal arising from physiological noise is usually located in the regions of the brain where neural activity does not occur, such as ventricles and large vessels (figure 1) (For more detail about defining noise components see [19, 20]).

The noise will not be present as the same component in each dataset because the artefacts are not spatially consistent. Therefore, the noise has to be identified and removed individually for each dataset. This can be done manually but to make this process much faster and less arbitrary it can be automated using software such as FIX [21] or AROMA-ICA [22].

FIX is an automated classification algorithm which uses training data from a subset of subjects from the current dataset to train a multi-level classifier to label signal and noise components in similar new datasets [21]. FIX requires training data as prior knowledge regarding what is signal and what is noise. There is a standard training data set available, but if the study is large enough it may be better to train a study-specific dataset on a subset of subjects as this training data may be more accurate at identifying

noise components in the given study. This method requires arbitrary judgement while creating the training dataset, but then it applies the same criteria to all the data in a study, which is more reliable than removing noise components from each dataset individually. FIX has been optimised for artefact removal from resting state network (RSN) data and is not currently recommended for event-related FMRI.

AROMA-ICA [22] is an alternative to FIX for event-related FMRI. It has been developed mainly to remove motion artefacts but it also removes some of the physiological noise. The advantage of AROMA-ICA is that it uses its own classifier and does not require creating a study-specific classifier.

If we have pulseoximeter and respiratory bellows data, it is possible to use both ICA denoising and the respiratory and cardiac recording [23]. However, there is an overlap between the cardio-respiratory signals and the ICA noise components which has to be accounted for. Typically, if physiological data were recorded during an event-related FMRI experiment, the time courses from a RETROICOR-type analysis can be used to regress out physiological signals from the data. This can either be done as a pre-processing step, or be incorporated in to a design matrix. The latter has the advantage of accounting for the loss of degrees of freedom as we include a large number of nuisance regressors.

As an example, figures 2-4 show data from a sensory stimulus in a healthy volunteer. Please note that a subject with relatively little motion was chosen. Figure 2 shows the results of modelling only the timing of the stimulus. The model fit is quite good (figure 2.B) and the max Z score is 10.55. If we add motion parameters and regress out the motion outliers the model becomes more complex (figure 3.A) and the max Z score is reduced (figure 3.B). This is because what might have been previously modelled as signal now has been regressed out as motion-related noise, but the model fit has improved (this is more apparent in figure 3.C which depicts a time course from a primary somatosensory (S1) ROI rather than the time course from the Zmax voxel in figure 3.B). Moreover, the small clusters of activation visible in figure 2.D, especially in the frontal lobes, are no longer present if motion is modelled (figure 3.D). Extension of the model to include data from physiological recordings further improves the model fit

(figure 4.C), and the activation map (more robust activation in insular and somatosensory cortices). The max Z score in the S1 ROI is also higher when the physiological data are modelled.

All of these corrections are predicated on the assumption that physiological data was actually collected to be used in the clean-up. However, many fMRI experiments are performed without acquisition of any physiological data at all. Recent research has suggested that it may still be possible to account for variations in physiology in these data both between sessions and between subjects [24, 25]. It is a common practice to apply a high-pass filter to functional time series during analysis, in order to remove what is generally referred to as “scanner drift”, i.e. the tendency for the resting signal to drift up or down over the course of an experiment [26, 27]. This is considered to be due to gradual changes in the hardware caused by heating. The cut-off frequency for this filter is usually determined by the lowest-frequency functional task or stimulus. These frequencies tend to be much lower for studies involving respiratory stimulus, where one period could be as long as 10 minutes, in contrast to cognitive tasks and stimuli, which tend to have periods of 1 minute or less.

Some of these low-frequency oscillations are caused by physiological changes and strongly correlate with heart rate and respiration rate. As both of these rates generally fall within defined bandwidths in the healthy population, it is possible to perform a Fourier transform on the 4D MRI data, and isolate these frequencies. The power at these frequencies in the time series may then either be removed, or more usefully, can be used to perform a kind of calibration to account for variations in blood volume or oxygen extraction fraction [25].

The advent of resting state fMRI showed that much of this “drift noise” is in fact genuine signal associated with activity in the brain [28], furthermore, there is some evidence that resting state networks have partially independent vascular and neuronal components [29]. It seems that much of the physiological impact on the resting state BOLD time series may actually be signals related to vascular networks [24, 30], and so careful consideration is needed before removing all physiological features of the resting state signal.

Sampling Respiratory Gases

When performing respiratory calibrated fMRI [31, 32], it is usual to collect oxygen and CO₂ traces. It is also common to collect respiratory and pulse data for physiological noise modelling. There are multiple ways of delivering respiratory gasses, and similarly many different ways to sample them, and the choice of one of these may significantly impact the other. In simplest terms, the main gas delivery options are: a mask, a cannula, or a mouthpiece. Each of these has its own strengths and weaknesses. From physiological monitoring perspective, the key element is to acquire accurate and easy to extract end-tidal values of oxygen and/or CO₂ (figure 5). This is often challenging because most methods of sampling respiratory gases, when used in combination with the delivery of gases (even just air), are susceptible to having the traces contaminated by either room air or the delivered gases. The main problem is that it is the very last bit of the exhaled gas of each breath that most closely reflects the alveolar partial pressures, and therefore, most closely matches the arterial partial pressures. However, the very end of a breath has very little force behind it, and thus is easily “blown back” by a constant stream of delivered gas, meaning the classic “end-tidal” point can be lost (figure 6.A).

A mouthpiece provides the easiest way to achieve a good seal for delivering gases, and a sample port directly at the mouth provides a very good trace. When combined with one-way valves, they add very little dead-space (volume of gas not involved with exchange in the lungs) to the breathing circuit. Moreover, there is almost no chance of contamination from room air, and with an open exhaust design of breathing circuit [33], little chance of contamination from delivered gases so the quality of the sample trace is excellent. The main drawback of a mouthpiece is that it is uncomfortable for the subject. Breathing exclusively through the mouth is not natural and causes distraction to some subjects. Moreover, breathing dry gas mixtures causes uncomfortable drying out of the mouth and gums, which is often exacerbated by the mouthpiece itself. This can result in the excess production of saliva causing increased swallowing which in turn leads to motion artefacts. Humidifying the gases reduces dryness, but if the moisture

levels are too high, it is unpleasant and may also result in an increase in swallowing, and achieving ideal humidity is difficult.

A full-face mask that covers both nose and mouth is probably the most common means of delivering gases to subjects in an FMRI experiment, and there is a broad range of designs available. Non-rebreathing masks provide the best control over the delivered gas mixture. Single-use non-rebreathing masks generally have one-way exhaust valves built into the body of the mask itself, whereas reusable masks tend to have a single large port for both inspiration and expiration. Masks invariably come with multiple issues that can impact their reliability, the main problem being leakage. Most mask designs make it difficult to obtain a tight seal against the face for every subject. Some people have faces that fit the shape of the mask exactly, but most people have funny noses, strange chins, weird cheekbones, or worst of all beards (hipsters are a significant problem). A room air leak will appear in a respiratory trace as a sudden drop in an elevated delivered gas towards the end of inspiration (figure 6.B), although this will usually not affect the measure of end-tidal values, it will result in poor control of the inspired fractions meaning that either the target level is missed, or that inspired levels have very high breath-by-breath variability. One approach to prevent this is not to rely on the mask to provide the seal, and rather to use tape or adhesive sheets to eliminate leakage [34]. This is undoubtedly effective, but it adds to the consumables costs, and marginally increases set-up time. Most subjects tolerate this well; however, anxious subjects may not be comfortable with it. And it may not work on bearded participants.

A nasal cannula can be used for sampling only, delivery only, or a two-tube cannula can deliver and sample gases simultaneously. Two-tube cannulas come in two types: the two-prong variety with one sampling prong and one delivery prong, and the two-prong, two-hole variety, which samples from both prongs, and delivers gases through holes at the base of the prongs. A delivery-only cannula is the simplest way to deliver gases to a subject but it offers little control over the inspired gas fractions and there is no way to measure inspired or expired gases. A two-tube cannula is less intrusive than a mask and is well tolerated by patients and anxious or slightly claustrophobic subjects. However, it offers far less control over inspired gas fractions, and the two-prong, two-hole variety can suffer from sampling contamination if the delivery holes are directed towards the

ends of the sampling prongs. The one-in, one-out two-prong cannula can be uncomfortable for subjects as a high-flow air blows directly up one nostril. Moreover, the sampling prong does not actually sample the delivered gas mixture as it is resting in the other nostril. This can result in very strange looking respiratory traces that are difficult to analyse. A sampling-only cannula can be useful for simple monitoring of respiratory gases for noise regression. It can also be used in combination with a mask to provide improved sampling during gas challenges but it will make it harder to get a perfect seal between the mask and the face. Interestingly, it is possible to achieve very good delivered fractions and end-tidal measurements when the exhaust valves in a non-rebreathing, bag-reservoir mask are taped closed, and a high flow-rate of over 15 litres per minute is used in combination with a sampling nasal cannula. This arrangement means that all excess and exhaled gases escapes via the edges of the mask, which prevents inflow of room air, but the pressure from the delivered gases is not sufficient to contaminate the sampled trace from the cannula. The added benefits of this arrangement is that it is very cheap, as it uses disposable components, and that there is no requirement of a good seal, and so is quick and easy to set up.

The next consideration is how to sample the gases. Many filters and connectors come with luer lock ports for attaching sample lines. Depending on the location and arrangement of delivery and exhaust valves, there is the potential that sampled gases may be contaminated by the delivered gas mixture. This will be more of a problem with closed breathing circuits such as those with a bag reservoir, as excess delivered gas exits the circuit via the mask, or at least past the sample port. Depending on the gas mix being delivered, this will have very different impacts on measured traces, some of which may be quite subtle and hard to spot. Contamination from delivered air (blowback) can result in a “shoulder” on the trace, eliminating the end-tidal points, via an increase in oxygen and a decrease in CO_2 (figure 7.A). Obviously, when using hyperoxic or hypercapnic mixtures, these effects will be larger, and hypercapnic mixtures will result in a positive spike in CO_2 that obscures the end-tidal point, rather than a decrease (figure 7.B). Similarly, an air leak into a mask during a hyperoxic stimulus will result in a downward spike in the oxygen trace at the end of the inhalation and may be mistaken for the end-tidal point because this point could now be the lowest point in the cycle (circled point in figure 6.B, although not low enough in this case to supplant the true

minimum). This will be interpreted, either during the study or analysis of the data, as the subject having a very low PaO_2 , when in fact, the PaO_2 may be quite adequate. It can be very difficult for either a human observer or software to accurately identify the true end-tidal oxygen value under these circumstances, but an approximation can often be obtained manually.

Gas analysis devices come in a variety of designs, however, they can be neatly divided into two groups depending on the number of pumps per gas being analysed. There can be one pump per gas, usually one for oxygen and one for CO_2 , or one pump for all gases. It may seem that more is better, but if two air pumps are connected to the same sample line, they must be carefully balanced so that they do not interfere with each other. If one pump has more drawing power, it can pull the gas out of the other pump's path. Very occasionally, if the two pumps have pulsatile air flows, then interference patterns can occur between them, causing a beating effect, which will be apparent in the measured data (figure 8). A similar effect may be due to a blockage in the line of one of the pumps, which could be internal to the pump itself and thus require the pump to be serviced. If the two pumps are drawing gases in at different speeds, this can cause a delay between the two traces, which can already be possible if the measurement techniques require different amounts of time. These effects would need to be measured and accounted for in the analysis.

There are several things to consider when setting up the gas analysers. Most data acquisition devices sample channels at a default frequency (often 1kHz) that is very high in comparison to the normal respiration rate ($\sim 0.2\text{Hz}$), which means that the acquired dataset is much larger than necessary. Generally, a frequency of 100Hz provides sufficient temporal resolution, and it may even be possible to obtain good quality data with a sampling rate as low as 10Hz, as this will still provide 50 to 100 points per cycle. It is worth noting that in addition, different gas sensors will have their own inherent response time that will limit the maximum rate of change they can detect, this is usually found in the hardware manual, and sampling at higher than this rate will not result in an actual increase in temporal resolution.

Once respiratory traces have been acquired they will require some pre-processing before being incorporated into any analysis. The nature of pre-processing depends on the objectives of the experiment. Extracting the end-tidal points from a full respiratory trace is the most commonly desired feature. With traces from air-only breathing, and from protocols with periods of hypercapnia or hyperventilation this is a relatively simple task which involves identifying the lowest point per breath from the oxygen trace and the highest point per breath of the CO₂ trace. As long as the time window is appropriate to encompass a complete respiration cycle this will provide a time course which is accurate, albeit with points somewhat randomly spread in time, with a low temporal resolution. Converting this time course into a regressor requires adjusting for the sampling delay, interpolating between the end-tidal points to create a full temporal resolution time course, and then using the scanner triggers to obtain estimates of the arterial partial pressure values at the time of each acquired volume, and down-sampling the time course to a list of these values. This process is made even more complicated by the inclusion of periods of hyperoxia. During the transition from normoxia to hyperoxia and during the hyperoxic period, the oxygen end-tidal points are the minima for each breath, however, during the transition between hyperoxia and normoxia, the oxygen end-tidal points become the maxima until they drop below the partial pressure of oxygen in the delivered air (figure 9). This requires very careful scripting to correctly extract these points; otherwise the transition will appear as a sudden drop to the oxygen value in the delivered air. This change is easy to determine by eye, but it is quite challenging to write a script that does this reliably for every subject.

The rate of decline in end-tidal oxygen levels is driven primarily by the total amount of oxygen dissolved in the tissues of the subject and their breathing rate, however a degree of this can also be due to dead-space. The inspired breaths include some of the previously expired breath, which has levels of oxygen above 20.7% (the normal level in air). As there is even dead space in the subject's own airways this is unavoidable, but it is advisable to minimize any additional dead space within the breathing circuit. Note that during the transition shown in figure 9, the inspired oxygen levels are slightly elevated and appear to decay exponentially down to the delivered level of 20.7%. In these data this is most likely due to the way in which the gases were delivered and sampled. A 2-tube nasal cannula delivering gases at 15 litres per minute will result in

gas building up in the bore of the magnet, after a switch from 100% oxygen to air it will take some time to clear the excess oxygen out of the bore. The fact that the subject is also exhaling oxygen levels above 20.7% will also slightly delay the return of inspired levels to that of the delivered air, as the bore itself becomes part of the dead space. In this case it takes approximately 5 breaths for the cloud of gas around the subject's face to reach the plateau, a delivery system with more tightly controlled gas delivery would not suffer from this effect to the same degree.

When using very high levels of inspired oxygen and T_2^* imaging there is the potential for susceptibility artefacts due to the paramagnetic gaseous molecular oxygen in the upper airways causing increased intravoxel dephasing in frontal areas of the brain [35]. This effect increases with inspired fraction of oxygen (FiO_2) and with field strength, so is of more concern at 7T. Hyperoxia also increases the levels of oxygen dissolved in the CSF, which can affect relaxation times and cause artefacts. If these effects are negatively impacting data, it may be necessary to mitigate this by decreasing the FiO_2 .

BOLD and ASL

The increased use of ASL sequences for both task-based fMRI and quantitative physiological measurements has required a re-evaluation of how to clean up a time series. In addition to the various possible readouts and k-space trajectories, there are four main types of ASL, namely: preparation pulsed ASL (PASL), continuous ASL (CASL), pseudo-continuous ASL (PCASL) and velocity-selective ASL (VS-ASL) [36]. Due to the differences in labelling location, and either spatial or temporal labelling width, each of these sequences interacts with the physiology in different ways, and thus is susceptible to artefacts or noise in different ways. With the growing popularity of PCASL, one of the most important considerations when using it in combination with hypercapnia or breath-hold experiments is the impact that these have on the inversion efficiency [16]. To further complicate matters, the relationship between flow velocity in the tagging arteries and inversion efficiency is non-linear, and due to the natural variations in the diameters of carotid and vertebral arteries, a hypercapnia-mediated increase in flow

velocity may potentially result in an increase in inversion efficiency in one vertebral artery and a concomitant decrease in the other. In order to accurately quantify regional cerebral blood flow (CBF), the experiment requires (1) performing a phase-contrast angiography scan of the tagging plane during both normo- and hypercapnia to establish the flow velocities in each of the four main arteries under each condition, (2) followed by a vessel-encoded PCASL (VEPCASL) scan [37] to determine the perfusion territories of each of these four arteries, and then finally (3) the hypercapnia fMRI scan, the results of which need to be scaled in each territory according to the inversion efficiency in each feeding artery. These scans would also all need to be planned with post-labelling delays appropriate for hypercapnia changing the arterial arrival times [38].

It has been shown that suppression of the background signal during ASL improves the SNR of the CBF measurements [39], and most implementations of both single and multiple post-labelling delay sequences now incorporate background suppression by default. Background suppression can either be directly applied, or, as in the case of Look-Locker sequences, it can be achieved inherently [40]. When combining ASL with BOLD the trade-off between the SNR of one versus the other must be considered. Recently, it has been demonstrated that as the SNR of ASL is much lower than the BOLD SNR, the BOLD SNR should always be sacrificed to improve ASL SNR. In particular, there had been concern that the use of background suppression during a combined BOLD/ASL sequence might destroy too much of the BOLD signal, and thus should not be used. This was shown not to be the case, and the current recommendation is that background suppression should always be used with ASL regardless whether we are interest in the simultaneous BOLD signal or not [41].

Simultaneous BOLD and ASL acquisition using echo planar imaging readouts (EPI), particularly for use with physiological models, increases the need for acquiring field maps to correct for susceptibility artefacts and signal dropout near air-tissue interfaces. The different echo times employed with the three non-intermediate-echo-time approaches, means that the distortions and dropout around the frontal and medial temporal regions are significantly different between the two data sets [42]. This effect should be considered even when only collecting BOLD data, but when the two datasets are mathematically incorporated into models, then the misalignment of voxels results in

significant errors in these regions, or at least unnecessary loss of data. Field map correction tools are included in the major functional analysis software packages, but are often not used by researchers, as they do not realise their importance.

Stimulus responses

It is worth mentioning that when analysing time-course data for respiratory stimuli, the standard task haemodynamic response function (HRF) is not appropriate. This is because the responses are not purely vascular in nature. The BOLD and ASL responses to hypercapnia follow the PaCO_2 , which for a 5% CO_2 in air mix takes approximately 1 minute to reach an effective plateau, although it can continue to rise gradually for several minutes [43]. The vascular response is driven by CO_2 levels in the arterioles and at precapillary sphincters, and thus is driven directly by the PaCO_2 . The time course for this change is determined by minute ventilation, cardiac output and total body blood volume. This can be modelled well using the Gamma function that is typical for HRF modelling (such as used by FEAT), with a standard deviation of 20 seconds and a mean lag of 30 seconds. For hyperoxia, the BOLD response is much slower, with FiO_2 levels between 0.75 and 1 taking around 2 minutes to plateau. It is best modelled using a standard deviation of 60 seconds and a mean lag of 60 seconds, the longer standard deviation relative to mean lag is due to the slower transitions than for CO_2 . The BOLD response to oxygen is passive and comes directly from the venous haemoglobin saturation levels, which are mediated by the PO_2 in the tissue. Thus the tissue acts as a buffer to changes, which results in longer wash-in and wash-out times.

In addition to the temporal characteristics of the fMRI signal changes, we regularly make the assumption that the relationship between stimulus magnitude and response magnitude is linear. In general, due to physical, chemical, or physiological constraints, most responses are sigmoidal. We usually work within a small range in the middle of this sigmoid and thus can approximate the relationships as linear. In reality however, the BOLD response to hyperoxia will plateau as the venous oxygen saturation (SvO_2) approaches 1.0, the CBF response to hypercapnia will similarly flatten as the dilatory capacity of the precapillary sphincters reach their minima or maxima. In situations of either extreme stimuli or in the presence of pathology, the assumption of linearity can

be violated [44]. Under such conditions, the BOLD and ASL responses to changes in end-tidal levels will either be muted, absent, or possibly even inverted, and thus cannot be accounted for using standard regressors. Respiratory stimuli and baseline-measure pilots can be used to determine if this is the case, and if so, only phase-based corrections should be applied, and a calibrated approach to the functional stimulus may be required.

Conclusions

It may seem that noise and confounds dominate the FMRI time series; however, it is impressive how robust and reliable both BOLD and ASL are at localising activation under these challenging conditions. The best defence against the various noise sources is to be aware of them, prevent artefacts in advance, pilot new studies, and determine which confounds are of sufficient magnitude to warrant addressing. There is also a real danger in doing too much. Overfitting can potentially result in more significant errors than a simple naïve analysis. This can be easily seen in the world of ICA, where using too many components results in meaningless patterns containing little power, but taken together result in pulling power from more important components. For example as a personal anecdote, I have included pulse triggers and respiratory belt information with PNM (<http://fsl.fmrib.ox.ac.uk/fsl/fslwiki/PNM>) [7], while also including end-tidal oxygen and CO₂ traces as parameter estimates for BOLD effects on ASL data, allowing for increases in oxygen to result in hyperventilation which would result in reduced blood flow and thus negative ASL signal from a reduced tag and control difference, only to discover that my data was fitted equally well by ignoring all of the extra information and simply applying a 10 second temporal filter to the raw tag and control data (TR = 4 seconds), and using an assumed HRF.

The most important thing to do is to look at your data. The time series of individual voxels or small ROI's will tell you much more about what is going on than an activation map. A voxel with an apparently great fit to the model, may have achieved this with substantial input from a temporal derivative term in order to account for a timing error, drawing power away from the parameter of interest. If the hypothesis being tested is only concerned with identifying regions of activation, then this may not matter,

however if the magnitude of BOLD signal changes is being used as part of calculating changes in metabolism via a physiological model, then this will significantly impact the final results. Even a matter as simple as checking the appropriateness of the HRF used is important, particularly in the case of breathing or gas paradigms, where in fact a *pulmonary response function* is required as the dynamics of the time course depend on the rate at which blood gases reach equilibrium, and hypercapnia, hyperoxia, breath holds, and hyperventilation all demonstrate very different dynamic behaviours, and are much slower than the HRF.

FMRI has become the dominant tool for imaging in neuroscience, and is rapidly encroaching into territory traditionally held by PET, CT, and ultrasound, but it is important to tread carefully when exploring new horizons as not all of the comfortable assumptions made at the outset will hold true under all conditions. The BOLD and ASL time courses are undoubtedly noisy, and there are tricks and tools for dealing with this, but no tool is a substitute for understanding the inherent behaviour of the brain, the scanner, and the analysis technique being employed.

Acknowledgements

The authors would like to thank the following organisations who provided funding for this work: EPSRC UK, MRC UK, CRUK. Thanks go also to Dr Hannah Hare, Dr Michael Germuska, and Dr Nicholas Blockley who aided in the accumulation of this wisdom.

References

- [1] M. Jenkinson, P. Bannister, M. Brady, S. Smith, Improved optimization for the robust and accurate linear registration and motion correction of brain images, *Neuroimage*, 17 (2002) 825-841.
- [2] K.J. Friston, S. Williams, R. Howard, R.S.J. Frackowiak, R. Turner, Movement-related effects in fMRI time-series, *Magn. Reson. Med.*, 35 (1996) 346-355.
- [3] C.F. Beckmann, S.M. Smith, Probabilistic Independent Component Analysis for Functional Magnetic Resonance Imaging, *IEEE Trans. Med. Imaging*, 23 (2004) 137-152.
- [4] M.J. McKeown, S. Makeig, G.G. Brown, T.P. Jung, S.S. Kindermann, A.J. Bell, T.J. Sejnowski, Analysis of fMRI data by blind separation into independent spatial components, *Hum. Brain Mapp.*, 6 (1998) 160-188.
- [5] P. Jezzard, R.S. Balaban, Correction for geometric distortion in echo planar images from B(o) field variations, *Magn. Reson. Med.*, 34 (1995) 65-73.
- [6] G.H. Glover, T.Q. Li, D. Ress, Image-based method for retrospective correction of physiological motion effects in fMRI: RETROICOR, *Magn. Reson. Med.*, 44 (2000) 162-167.

- [7] J.C.W. Brooks, C.F. Beckmann, K.L. Miller, R.G. Wise, C.A. Porro, I. Tracey, M. Jenkinson, Physiological noise modelling for spinal functional magnetic resonance imaging studies, *Neuroimage*, 39 (2008) 680-692.
- [8] F.C. Moreton, K.A. Dani, C. Goutcher, K. O'Hare, K.W. Muir, Respiratory challenge MRI: Practical aspects, *NeuroImage: Clinical*, 11 (2016) 667-677.
- [9] D.F. Treacher, R.M. Leach, ABC of oxygen: Oxygen transport - 1. Basic principles, *Br. Med. J.*, 317 (1998) 1302-1306.
- [10] R.G. Wise, K. Ide, M.J. Poulin, I. Tracey, Resting fluctuations in arterial carbon dioxide induce significant low frequency variations in BOLD signal, *Neuroimage*, 21 (2004) 1652-1664.
- [11] R.M. Birn, M.A. Smith, T.B. Jones, P.A. Bandettini, The Respiration Response Function: The temporal dynamics of fMRI signal fluctuations related to changes in respiration, *Neuroimage*, 40 (2008) 644-654.
- [12] W. Huijbers, C.M.A. Pennartz, E. Beldzik, A. Domagalik, M. Vinck, W.F. Hofman, R. Cabeza, S.M. Daselaar, Respiration phase-locks to fast stimulus presentations: implications for the interpretation of posterior midline "deactivations", *Hum. Brain Mapp.*, 35 (2014) 4932-4943.
- [13] J.P. Farthing, J. Cummine, R. Borowsky, P.D. Chilibeck, G. Binsted, G.E. Sarty, False activation in the brain ventricles related to task-correlated breathing in fMRI speech and motor paradigms, *Magnetic Resonance Materials in Physics, Biology and Medicine*, 20 (2007) 157-168.
- [14] C. Chang, J.P. Cunningham, G.H. Glover, Influence of heart rate on the BOLD signal: The cardiac response function, *Neuroimage*, 44 (2009) 857-869.
- [15] H.V. Hare, M. Germuska, M.E. Kelly, D.P. Bulte, Comparison of CO₂ in air versus carbogen for the measurement of cerebrovascular reactivity with magnetic resonance imaging, *J. Cereb. Blood Flow Metab.*, 33 (2013) 1799-1805.
- [16] S. Aslan, F. Xu, P.L. Wang, J. Uh, U.S. Yezhuvath, M. Van Osch, H. Lu, Estimation of labeling efficiency in pseudocontinuous arterial spin labeling, *Magn. Reson. Med.*, 63 (2010) 765-771.
- [17] Z. Chen, X. Zhang, C. Yuan, X. Zhao, M.J.P. van Osch, Measuring the labeling efficiency of pseudocontinuous arterial spin labeling, *Magn. Reson. Med.*, DOI 10.1002/mrm.26266(2016) n/a-n/a.
- [18] Y. Li, D. Mao, H. Lu, Cardiac-triggered pCASL: A cost-effective scheme to enhance the SNR of ASL, *Proc. Intl. Soc. Mag. Reson. Med.*, 2015, pp. 2961.
- [19] R.E. Kelly, G.S. Alexopoulos, Z. Wang, F.M. Gunning, C.F. Murphy, S.S. Morimoto, D. Kanellopoulos, Z. Jia, K.O. Lim, M.J. Hoptman, Visual inspection of independent components: Defining a procedure for artifact removal from fMRI data, *J. Neurosci. Methods*, 189 (2010) 233-245.
- [20] C.F. Beckmann, M. DeLuca, J.T. Devlin, S.M. Smith, Investigations into resting-state connectivity using independent component analysis, *Philosophical Transactions of the Royal Society B: Biological Sciences*, 360 (2005) 1001.
- [21] L. Griffanti, G. Salimi-Khorshidi, C.F. Beckmann, E.J. Auerbach, G. Douaud, C.E. Sexton, E. Zsoldos, K.P. Ebmeier, N. Filippini, C.E. Mackay, S. Moeller, J. Xu, E. Yacoub, G. Baselli, K. Ugurbil, K.L. Miller, S.M. Smith, ICA-based artefact removal and accelerated fMRI acquisition for improved resting state network imaging, *Neuroimage*, 95 (2014) 232-247.

- [22] R.H.R. Pruim, M. Mennes, D. van Rooij, A. Llera, J.K. Buitelaar, C.F. Beckmann, ICA-AROMA: A robust ICA-based strategy for removing motion artifacts from fMRI data, *Neuroimage*, 112 (2015) 267-277.
- [23] O.K. Faull, M. Jenkinson, M. Ezra, K.T.S. Pattinson, Conditioned respiratory threat in the subdivisions of the human periaqueductal gray, *eLife*, 5 (2016).
- [24] A.M. Golestani, L.L. Wei, J.J. Chen, Quantitative mapping of cerebrovascular reactivity using resting-state BOLD fMRI: Validation in healthy adults, *Neuroimage*, 138 (2016) 147-163.
- [25] S.M. Kazan, S. Mohammadi, M.F. Callaghan, G. Flandin, L. Huber, R. Leech, A. Kennerley, C. Windischberger, N. Weiskopf, Vascular autorescaling of fMRI (VasA fMRI) improves sensitivity of population studies: A pilot study, *Neuroimage*, 124, Part A (2016) 794-805.
- [26] A.M. Smith, B.K. Lewis, U.E. Ruttimann, F.Q. Ye, T.M. Sinnwell, Y. Yang, J.H. Duyn, J.A. Frank, Investigation of low frequency drift in fMRI signal, *Neuroimage*, 9 (1999) 526-533.
- [27] L. Yan, Y. Zhuo, Y. Ye, S.X. Xie, J. An, G.K. Aguirre, J. Wang, Physiological origin of low-frequency drift in blood oxygen level dependent (BOLD) functional magnetic resonance imaging (fMRI), *Magn. Reson. Med.*, 61 (2009) 819-827.
- [28] K. Murphy, R.M. Birn, P.A. Bandettini, Resting-state fMRI confounds and cleanup, *Neuroimage*, 80 (2013) 349-359.
- [29] Y. Tong, L.M. Hocke, X. Fan, A.C. Janes, B. deB Frederick, Can apparent resting state connectivity arise from systemic fluctuations?, *Frontiers in Human Neuroscience*, 9 (2015).
- [30] M.G. Bright, K. Murphy, Is fMRI "noise" really noise? Resting state nuisance regressors remove variance with network structure, *Neuroimage*, 114 (2015) 158-169.
- [31] T.L. Davis, K.K. Kwong, R.M. Weisskoff, B.R. Rosen, Calibrated functional MRI: Mapping the dynamics of oxidative metabolism, *Proc. Natl. Acad. Sci. U. S. A.*, 95 (1998) 1834-1839.
- [32] P.A. Chiarelli, D.P. Bulte, R. Wise, D. Gallichan, P. Jezzard, A calibration method for quantitative BOLD fMRI based on hyperoxia, *Neuroimage*, 37 (2007) 808-820.
- [33] F.B. Tancredi, I. Lajoie, R.D. Hoge, A simple breathing circuit allowing precise control of inspiratory gases for experimental respiratory manipulations, *BMC Research Notes*, 7 (2014).
- [34] C.I. Mark, M. Slessarev, S. Ito, J. Han, J.A. Fisher, G.B. Pike, Precise control of end-tidal carbon dioxide and oxygen improves BOLD and ASL cerebrovascular reactivity measures, *Magn. Reson. Med.*, 64 (2010) 749-756.
- [35] D.T. Pilkinton, S.R. Gaddam, R. Reddy, Characterization of paramagnetic effects of molecular oxygen on blood oxygenation level-dependent-modulated hyperoxic contrast studies of the human brain, *Magn. Reson. Med.*, 66 (2011) 794-801.
- [36] J.M. Pollock, H. Tan, R.A. Kraft, C.T. Whitlow, J.H. Burdette, J.A. Maldjian, Arterial Spin Labeled MRI Perfusion Imaging: Clinical Applications, *Magn. Reson. Imaging Clin. N. Am.*, 17 (2009) 315-338.
- [37] E.S.K. Berry, P. Jezzard, T.W. Okell, An Optimized Encoding Scheme for Planning Vessel-Encoded Pseudocontinuous Arterial Spin Labeling, *Magn. Reson. Med.*, 74 (2015) 1248-1256.
- [38] D.C. Alsop, J.A. Detre, X. Golay, M. Günther, J. Hendrikse, L. Hernandez-Garcia, H. Lu, B.J. Macintosh, L.M. Parkes, M. Smits, M.J.P. Van Osch, D.J.J. Wang, E.C. Wong, G. Zaharchuk, Recommended implementation of arterial spin-labeled Perfusion mri for clinical applications: A consensus of the ISMRM Perfusion Study group and the European consortium for ASL in dementia, *Magn. Reson. Med.*, 73 (2015) 102-116.

- [39] K.S. St. Lawrence, J.A. Frank, P.A. Bandettini, F.Q. Ye, Noise reduction in multi-slice arterial spin tagging imaging, *Magn. Reson. Med.*, 53 (2005) 735-738.
- [40] M. Gunther, M. Bock, L.R. Schad, Arterial spin labeling in combination with a look-locker sampling strategy: Inflow turbo-sampling EPI-FAIR (ITS-FAIR), *Magn. Reson. Med.*, 46 (2001) 974-984.
- [41] E. Ghariq, M.A. Chappell, S. Schmid, W.M. Teeuwisse, M.J.P. van Osch, Effects of background suppression on the sensitivity of dual-echo arterial spin labeling MRI for BOLD and CBF signal changes, *Neuroimage*, 103 (2014) 316-322.
- [42] M.L. Gorno-Tempini, C. Hutton, O. Josephs, R. Deichmann, C. Price, R. Turner, Echo time dependence of BOLD contrast and susceptibility artifacts, *Neuroimage*, 15 (2002) 136-142.
- [43] M.J. Poulin, P.J. Liang, P.A. Robbins, Dynamics of the cerebral blood flow response to step changes in end- tidal PCO₂ and PO₂ in humans, *J. Appl. Physiol.*, 81 (1996) 1084-1095.
- [44] O. Sobczyk, A. Battisti-Charbonney, J. Fierstra, D.M. Mandell, J. Poublanc, A.P. Crawley, D.J. Mikulis, J. Duffin, J.A. Fisher, A conceptual model for CO₂-induced redistribution of cerebral blood flow with experimental confirmation using BOLD MRI, *Neuroimage*, 92 (2014) 56-68.

Figure Captions

Figure 1. Component from ICA analysis related to physiological noise. A. Spatial map showing a characteristic distribution near the large vessels and ventricles. B. Time course of the same component with an oscillatory pattern without big spikes. C. Power spectrum of the time course with a peak around 0.1 Hz corresponding to an aliased cardiac signal [20].

Figure 2. A. Basic design modelling only the timing of experimental stimuli. B. Time series from Zmax voxel. C. Time series from bilateral primary somatosensory cortex ROI. D. Z-stats map thresholded at 2.3.

Figure 3. A. Alternative/Extended design with extended motion parameters, and motion outliers, but without modelling of cardiac and respiratory parameters. B. Time series from Zmax voxel. C. Time series from bilateral primary somatosensory cortex ROI. D. Z-stats map thresholded at 2.3.

Figure 4. A. Alternative/Extended design with extended motion parameters, motion outliers and cardiac and respiratory parameters from the traces recorded during the scan. Please note that we are still only interested in the activation correlating with the task/experimental events. B. Time series from Zmax voxel. C. Time series from bilateral primary somatosensory cortex ROI. D. Z-stats map thresholded at 2.3.

Figure 5. “Perfect” respiratory traces showing a classic ramp to the end-tidal point. This effectively tracks the gradient in gas partial pressures from the mouth to the alveolar.

Figure 6. A. Contamination caused by blowback on a CO₂ trace during delivery of air with a mask. The tell-tale “shoulder” in the circle is the typical characteristic. The sample is contaminated by the delivered gases as they have a higher pressure than the end of the expired breath at the sample location. An approximation of the true end-tidal value can be obtained from the point indicated with the arrow, but it will be slightly lower than the true value. The oxygen trace would look the same only inverted. B. Mask leak during hyperoxia. The leak is shown by the circle. In this case the true end-tidal point shown by the arrow is still easily extractable, it is just lower than it would be without the leak. The situation is much worse however if the leak is more severe, as the low point of the leak will be lower than the end-tidal point, and thus will be readily mistaken as such by both humans and analysis scripts.

Figure 7. A. Blowback with a 2-tube nasal cannula, showing lowering of the CO₂ trace towards the end of the breath while on air (left ellipse), and a spike during hypercapnia (right circle). Delivered gas was 10% CO₂ to achieve a ~5% inspired fraction once mixed with room air during the inhalation. Best approximations of end-tidal values can be manually extracted at the points indicated by the arrows. B. Zooming in on a more extreme example of blowback during hypercapnia. The left circle shows blowback at the end of expiration, obscuring the true end-tidal point. The right circle shows blowback at the end of inspiration. The “true” trace is indicated by the purple line.

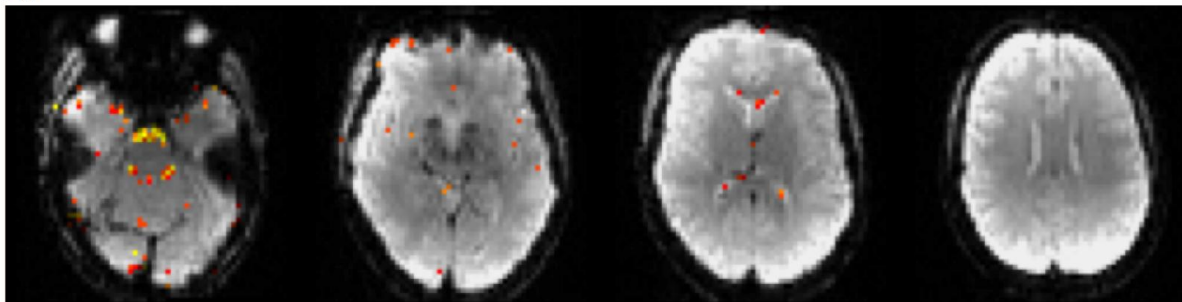
Figure 8. Two pulsatile pumps interfering with each other. The high frequency oscillations in the traces are a result of a pressure wave surging back and forth between

the 2 pumps. The 2 traces are also badly out of synch as the maxima of one should coincide with the minima of the other.

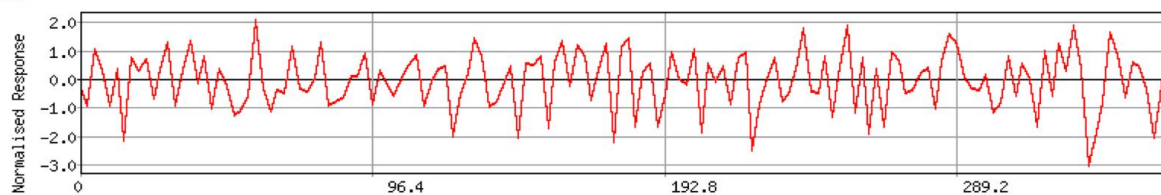
Figure 9. Oxygen trace during a mild hyperoxic stimulus showing the end-tidal time course in green. The circle shows the period during the transition from hyperoxia to normoxia where the end-tidal points become the local maxima rather than the local minima.

fig. 1

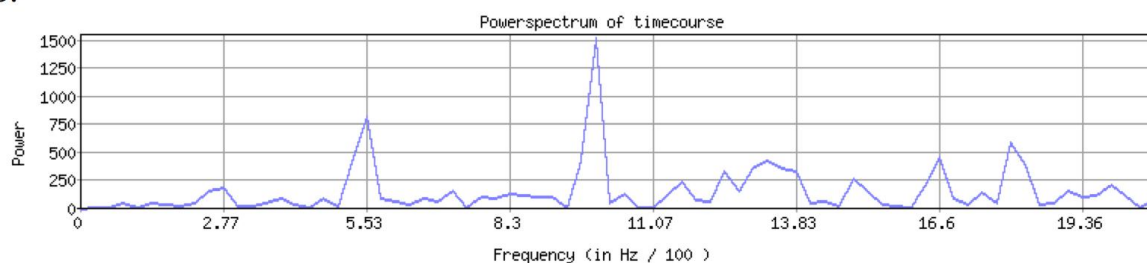
A.



B.



C.



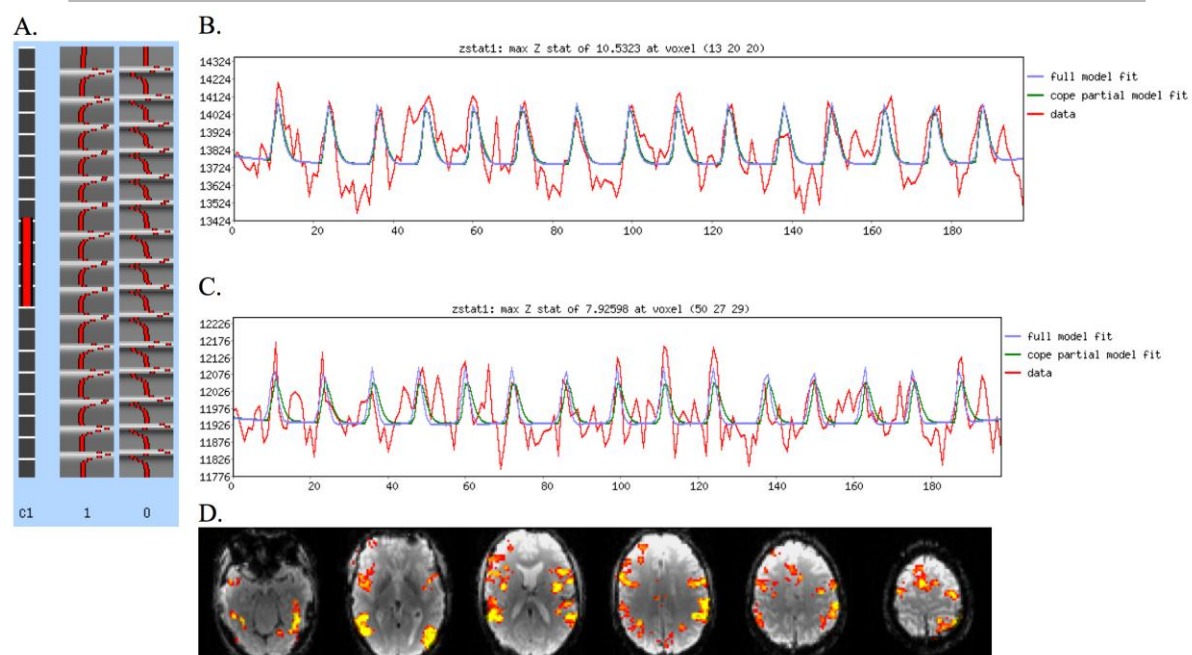
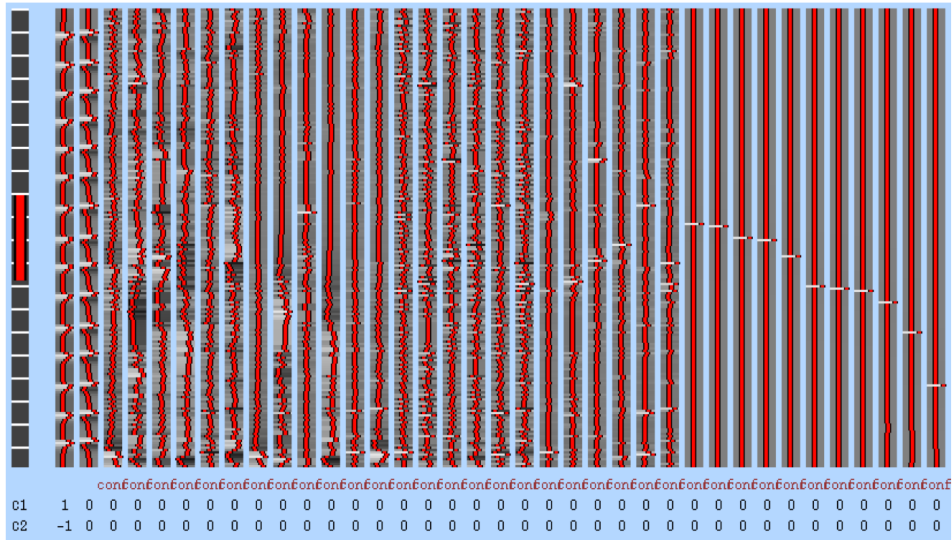
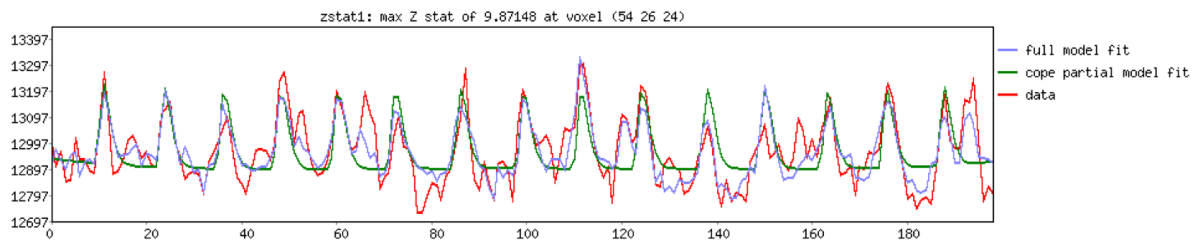


Fig. 3

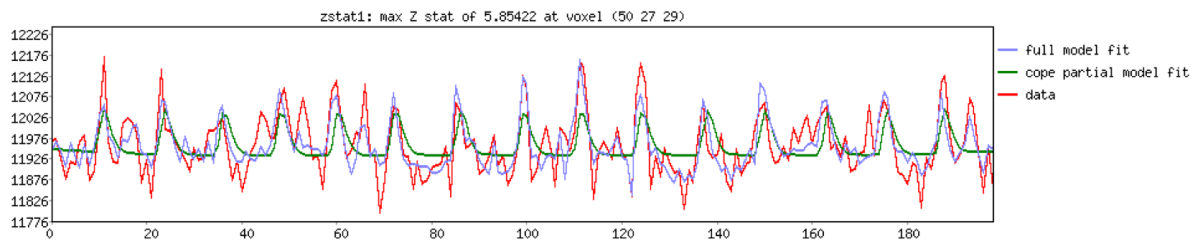
A.



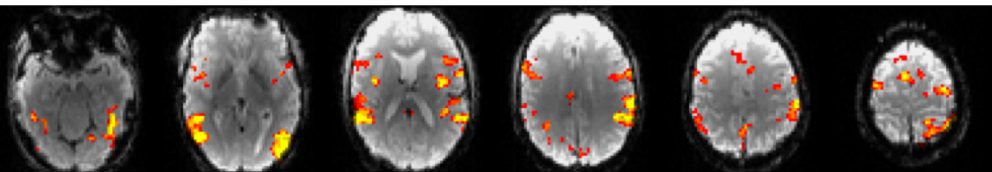
B.



C.



D.



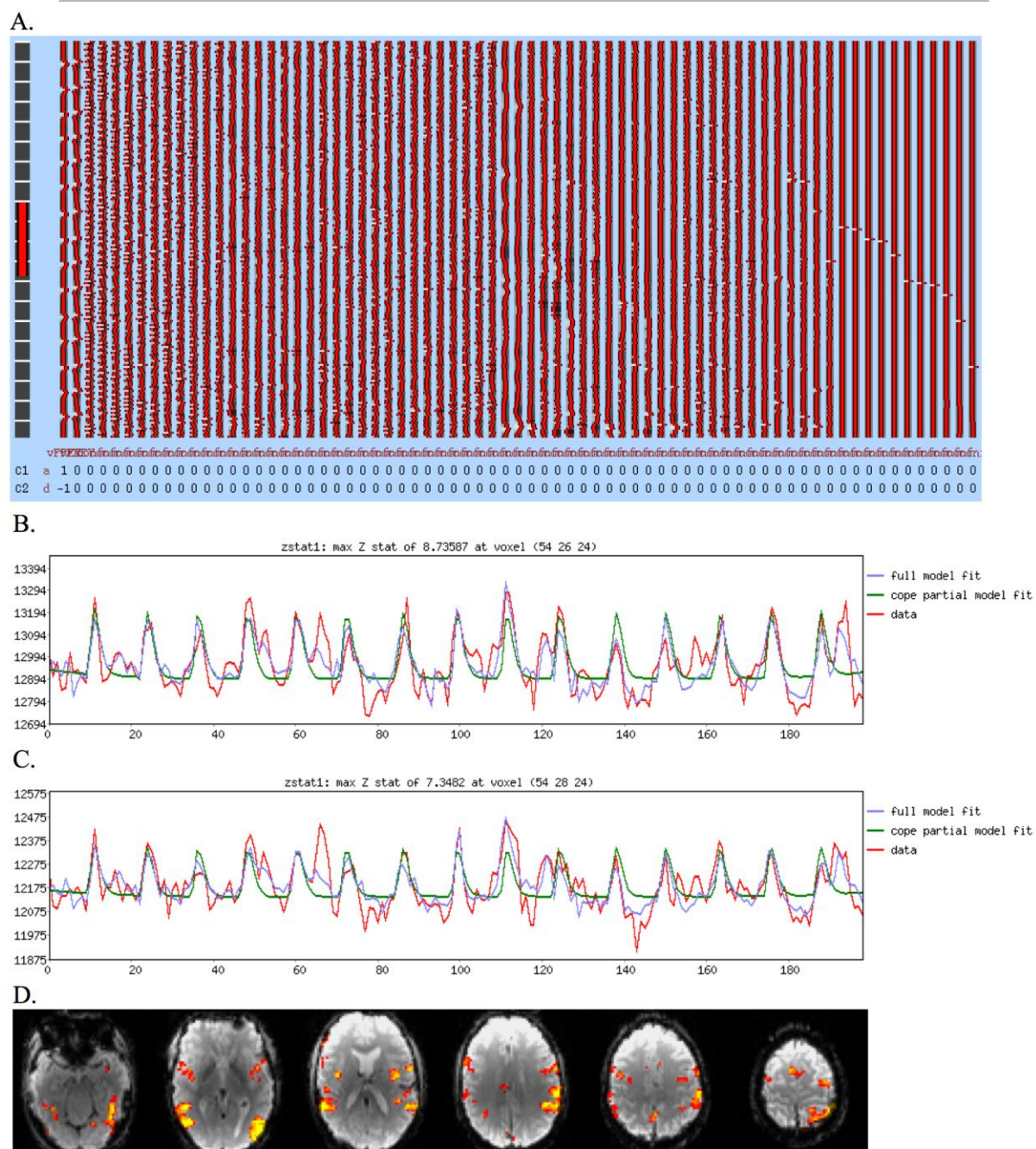


fig. 5

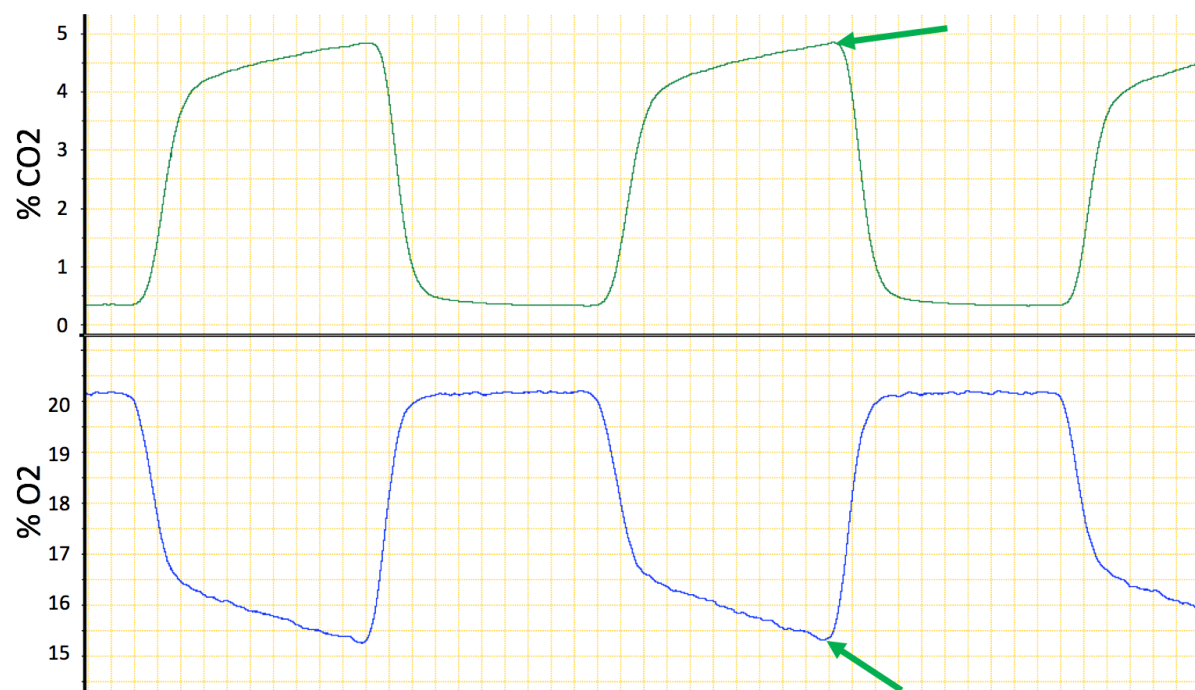


fig 6

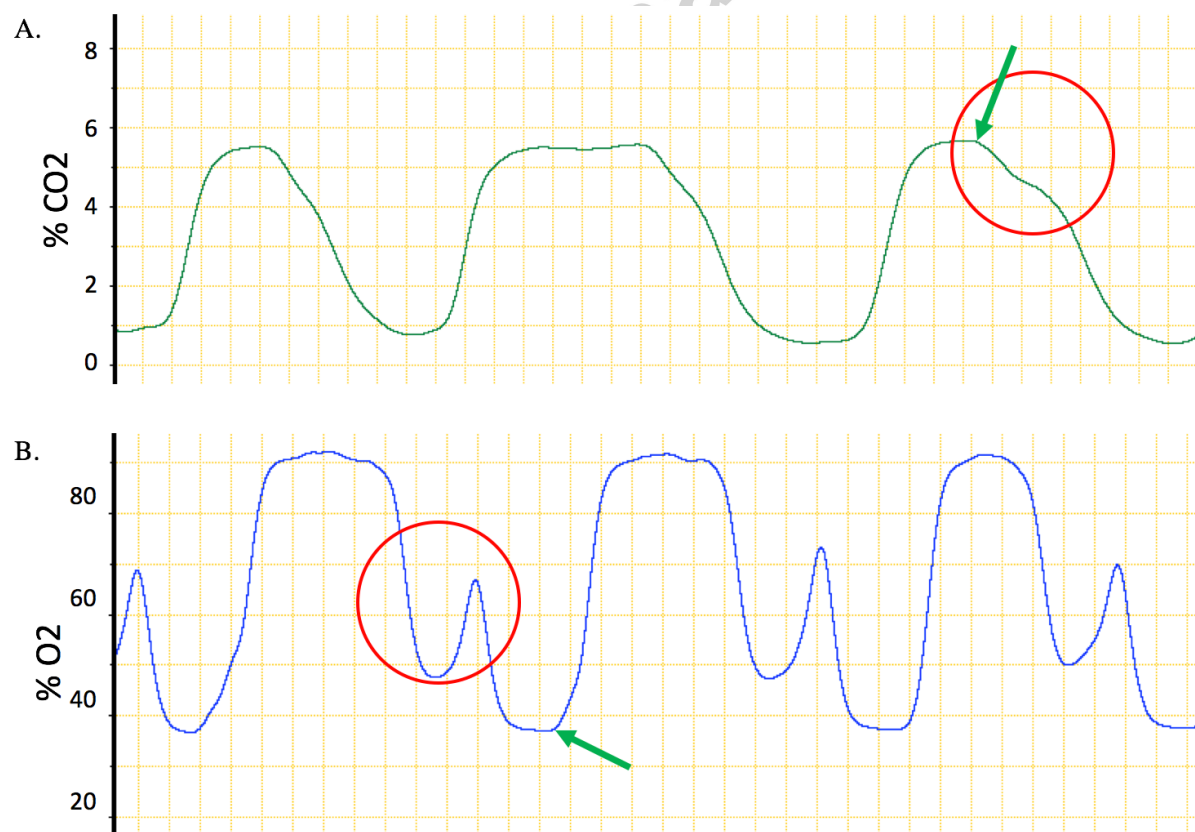


fig 7

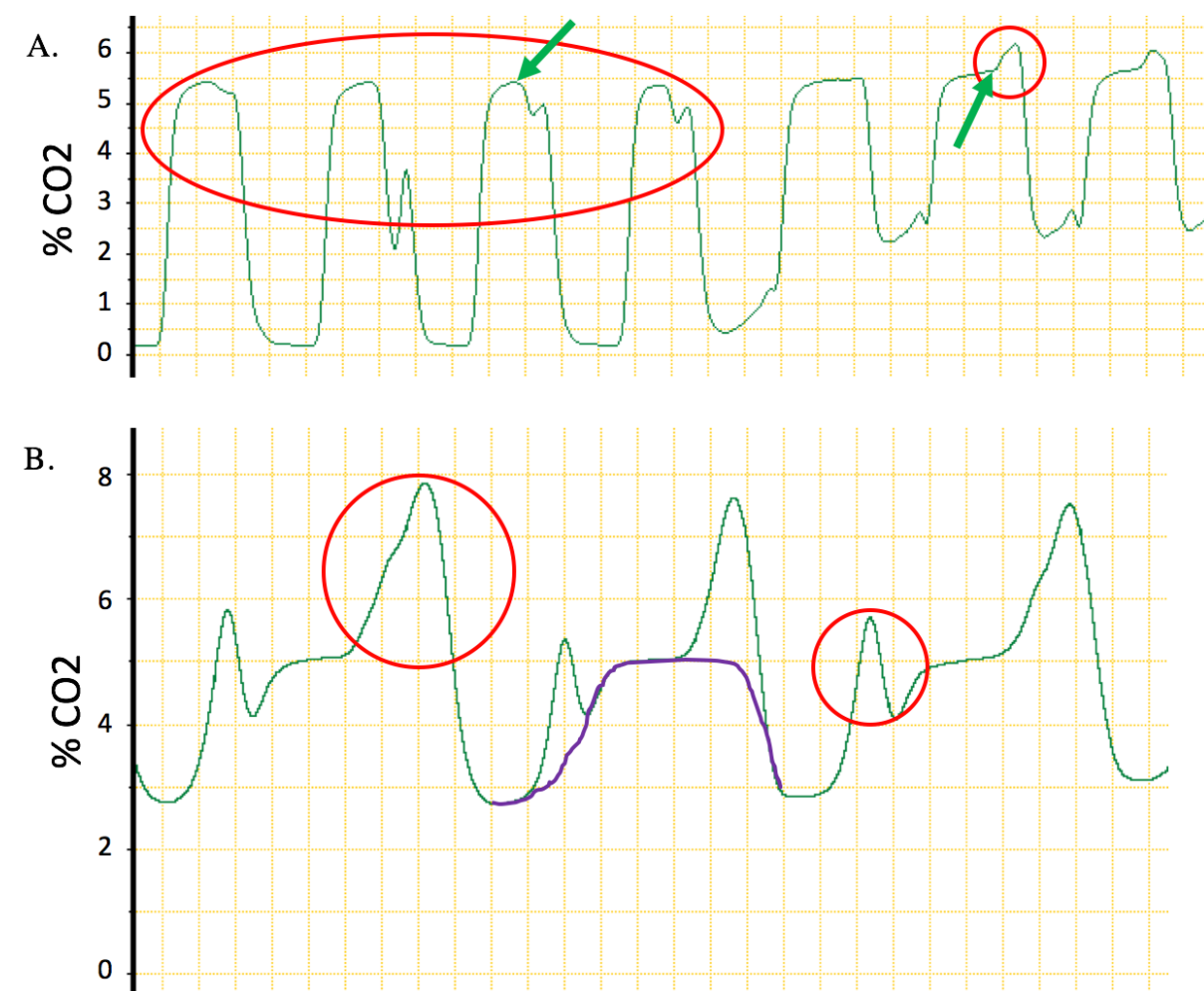


fig 8

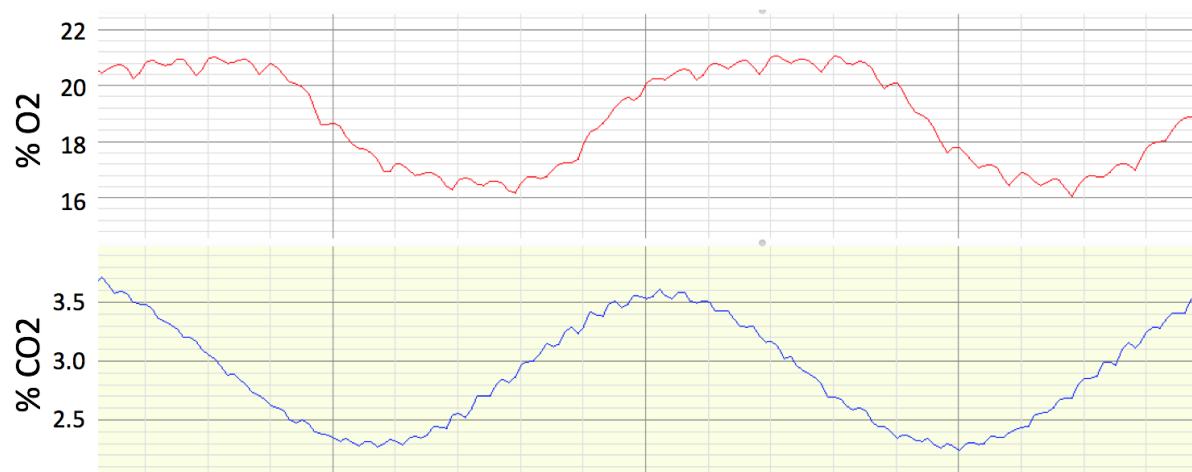


fig 9

